

# Anomalous roughening of wood fractured surfaces

Stéphane Morel,<sup>1</sup> Jean Schmittbuhl,<sup>2</sup> Juan M. López,<sup>3</sup> and Gérard Valentin<sup>1</sup>

<sup>1</sup> *Lab. de Rhéologie du Bois de Bordeaux, UMR 123, Domaine de l'Hermitage, B.P.10, 33610 Cestas Gazinet, France*

<sup>2</sup> *Lab. de Géologie, URA 1316, Ecole Normale Supérieure, 24 rue Lhomond, 75231 Paris Cedex 05, France*

<sup>3</sup> *Department of Mathematics, Imperial College, 180 Queen's Gate, London SW7 2BZ, United Kingdom*

Scaling properties of wood fractured surfaces are obtained from samples of three different sizes. Two different woods are studied: Norway spruce and Maritime pine. Fracture surfaces are shown to display an anomalous dynamic scaling of the crack roughness. This anomalous scaling behavior involves the existence of two different and independent roughness exponents. We determine the local roughness exponents  $\zeta_{loc}$  to be 0.87 for spruce and 0.88 for pine. These results are consistent with the conjecture of a universal local roughness exponent. The global roughness exponent is different for both woods,  $\zeta = 1.60$  for spruce and  $\zeta = 1.35$  for pine. We argue that the global roughness exponent  $\zeta$  is a good index for material characterization.

## I. INTRODUCTION

Since the pioneering work of Mandelbrot *et. al.* [1], it has been firmly established that topography of fracture surfaces exhibits remarkable scaling properties. A fracture surface  $z(x, y)$  is statistically invariant under an anisotropic scaling transformation:

$$(x, y, z) \rightarrow (\lambda x, \lambda y, \lambda^\zeta z) \quad (1)$$

where  $\zeta$  is the *roughness exponent*. Experimental results obtained on various materials (steels [1], glass [2], rocks [3,4], ceramics [5,6], metallic alloys [6–8] and aluminium alloys [9,10]), both fragile and ductile, have shown that the roughness exponent  $\zeta$  is found between 0.7 and 0.9 (see [11] for a recent review). The robustness of the results seems to support the idea suggested by Bouchaud *et. al.* [10] that  $\zeta \simeq 0.8$  might be a universal value of the roughness exponent, *i.e.*, independent of the material properties. This conjecture implies that the fracture toughness is not correlated to the roughness exponent  $\zeta$ . However, morphology of fracture surfaces seems to be affected by material properties.

It has been suggested by Bouchaud *et. al.* [12] that models of front lines propagating through randomly distributed impurities [13–15] might be relevant to understand the morphology of the fracture surfaces [16,17]. The development of the fracture roughness has been described as a Family-Vicsek scaling [18,3]. However, in a very recent experimental study [19], it has been found that the surface of a brittle fracture in a granite block exhibited anomalous dynamic scaling properties akin to what occurs in some models of nonequilibrium kinetic roughening [20–24].

The anomalous scaling is defined as follows. The development of the fluctuations of the height  $h(x, t)$  with time is characterized by the root mean square  $w(l, t)$  at time  $t$  over a window size  $l$  along the  $x$ -axis (perpendicular to the propagation direction)

$$w(l, t) = \left\langle \frac{1}{l} \sum_{i=1}^l h(x_i, t)^2 - \left( \frac{1}{l} \sum_{i=1}^l h(x_i, t) \right)^2 \right\rangle_j^{1/2} \quad (2)$$

where the brackets  $\langle \dots \rangle_j$  denotes an average over the window position  $j$ . The roughness  $w(l, t)$  is expected to scale in the case of anomalous scaling as [24]

$$w(l, t) \sim \begin{cases} t^{\beta_*} l^{\zeta_{loc}} & \text{if } l \ll t^{1/z} \\ t^{\zeta/z} & \text{if } l \gg t^{1/z} \end{cases} \quad (3)$$

where the exponent  $\beta_* = (\zeta - \zeta_{loc})/z$  is an anomalous time exponent. This anomalous dynamic scaling involves two different and independent roughness exponents: the local roughness exponent  $\zeta_{loc}$ , which describes the scaling when one considers windows smaller than the system size, and the global exponent  $\zeta$  for scaling involving the system size [24]. The local roughness exponent  $\zeta_{loc}$  is actually at reach of the methods currently used for experiment analyses. The global exponent  $\zeta$  is more difficult to extract from a classical roughness measurement. Both exponents have to be taken into account for a complete description of the scaling behavior of the surface. According to Eq. (3), the correlation length  $\xi(t) \sim t^{1/z}$  corresponds to a characteristic length below which the surface appears as self-affine with the local exponent  $\zeta_{loc}$ .

In Ref. [19], global and local roughness exponents,  $\zeta = 1.2$  and  $\zeta_{loc} = 0.79$  respectively, have been measured. The latter study was performed on a mechanically isotropic material (granite). However, many materials have anisotropic mechanical properties like wood, reinforced concrete and most composite materials. Anisotropic properties result generally from structural reinforcements along specific directions. It is of great interest to understand how fractures in such materials are influenced by the anisotropic texture.

In this study, we determine the complete scaling behavior of the fracture roughness resulting from stable crack propagation in wood samples of different sizes. For two different woods (Maritime pine and Norway spruce), we show that the local fluctuations of crack surfaces exhibit anomalous dynamic scaling properties. The global roughness exponent is different for both woods. Local roughness exponents are identical for both woods and support the conjecture of a universal local roughness exponent for brittle fracture surfaces. The main consequence of

this anomalous scaling is that the magnitude of the surface fluctuations over regions is not just a function of the region size but also of the system size.

The paper is organized as follows. In Sec. II we describe experimental setups for crack propagation and fracture surface measurement. Section III is devoted to the anomalous dynamic scaling behavior. In Sec. IV, we study the roughness magnitude as function of the system size. Finally, we discuss implications for fracture process in Sec. V.

## II. EXPERIMENT

Wood is a natural material which displays a structural anisotropy resulting from the presence of running cells in the radial direction. Two commercially wood species have been tested : Maritime pine (*Pinus pinaster Ait*) and Norway spruce (*Picea abies L.*). Pine specimens have an average oven dry specific weight ( $\rho$ ) of 560 kg/m<sup>3</sup> and growth rings are approximately 4 mm wide. Typical values for spruce specimens are: ( $\rho$ ) = 390 kg/m<sup>3</sup> and growth rings of 2 to 5 mm wide. Moisture content of all specimens was measured between 11 and 13 %.

Crack surfaces are obtained from a modified Tapered Double Cantilever Beam (TDCB) specimens. A fracture was initiated from a straight notch machined with a band saw (thickness 2 mm) and prolonged on few millimeters with a razor blade (thickness 0.2 mm). Fracture is obtained through uniaxial tension with a constant opening rate (Fig.1). The tapered shape of the specimens allows to obtain a mode I stable crack growth (see Ref. [25] for details) which induces a constant crack speed. The crack speed was around 0.6 mm/s (from 0.3 mm/s for small specimens to 1mm/s for large specimens). Crack surfaces were generated along an average radial-longitudinal plane by aligning the growth rings perpendicular to the straight notch. In order to obtain an evolution of the amplitude of the roughness as function of the system size, three geometrically similar specimens of sufficiently different sizes have been fractured. We used samples of size  $L$  equal to 11.25, 30, and 60 mm (see Fig.1).

Anatomical characteristics of wood introduce typical scales which might appear as cutoffs for scale invariances. Most tetragonal tracheid cells in pine and spruce are about 25  $\mu$ m wide. During loading cell walls break revealing U-shaped profiles with rugged edges because of the rectangular shape of the tracheid section. Thickness of cell walls varies from 2 to 10  $\mu$ m. This facies of fracture surface is characteristic of a local brittle fracture process.

Topographies of the crack surfaces were recorded with a mechanical profiler along regular grids. Grid axes are along the  $x$  direction which is parallel to the initial notch and along the  $y$  direction which is the crack propagation direction (Fig.1). The step of sampling in the  $x$  direction is adjusted to the minimum cell width :  $\Delta x = 25 \mu$ m and to the cell length in the  $y$  direction :  $\Delta y = 2.5$  mm.

Profiles along the  $x$ -axis were sampled with 2050 points for specimens of width  $L = 60$  mm, 1030 points for specimens of width  $L = 30$  mm, and 360 points for specimens of width  $L = 11.25$  mm. For each map, the first profile ( $y = 0$ ) is sampled in the immediate vicinity of the initial straight notch and has a zero roughness. As the distance  $y$  to the notch increases, the roughness develops up to 3 mm. The vertical resolution is estimated from the height differences between two successive sampling along the same line. Its magnitude is about 3  $\mu$ m. Horizontal resolutions along  $x$  and  $y$ -axis are about 5  $\mu$ m. In the case of pine an additional specimen size was tested :  $L = 22.50$  mm with 800 points, but only profiles far from the notch have been recorded. Table I lists parameters of the various studied samples.

## III. ANOMALOUS DYNAMIC SCALING

As mentioned above, fractures of all specimens have been obtained at constant crack speed. Subsequently, we assumed a linear relationship between the  $y$ -position of the profiles and the crack propagation time  $t$ . Height profiles are considered as descriptions of the advancing crack front  $h(x, t)$ . Complete spatio-temporal evolution of the crack front can thus be produced from roughness maps.

In Figure 2, we present the development of the roughness  $w(l, t)$  versus time  $t$  in a log-log plot for different window sizes  $l$  in the case of the spruce specimen (s60-1) which is 60 mm wide. The upper line is a fit of the roughness growth for the largest window size ( $l = 13.975$  mm). The slope of this fit provides an estimate of the ratio of the global roughness exponent and the dynamical exponent :  $\zeta/z \approx 0.26$ . The fit is computed for times between time  $t_{min}$  and time  $t_{max}$ . Before time  $t_{min}$  the crack speed is not constant. After time  $t_{max}$ , the roughness has saturated because of the reach of the system size.

The lower line is a fit of the roughness measured for a small window size ( $l = 0.175$  mm). It appears that  $w(l, t)$  increases like a power law as a function of the crack propagation time  $t$  even for small window sizes. The slope of the fit is 0.14 significantly larger than zero and gives an estimate of the  $\beta_*$  exponent. This unconventional dependence on time is an illustration of the anomalous scaling and differ from a Family-Vicsek scaling where the roughness is expected to be time independent for small window sizes.

These two regimes are in good agreement with the anomalous scaling proposed in Eq.(3). A similar behavior has been observed for all specimens.

## A. Local roughness exponent

The local roughness exponent  $\zeta_{loc}$  is determined using four methods: the variable bandwidth methods : root mean square and max-min difference [3,28], the power spectrum and the averaged wavelet coefficient method [27]. Local roughness exponents  $\zeta_{loc}$  have been determined on profiles located far from the notch, *i.e.*, at long times. Results on specimen s60-1 are used as illustrations. Complete results for all specimens are provided in Table I.

In the root mean square method, the roughness  $w$  over a window  $l$  is expected from Eq.(2) to scale at long enough time as

$$w(l, t \gg l^{1/z}) \sim l^{\zeta_{loc}} \quad (4)$$

From Figure 3 the local roughness exponent is :  $\zeta_{loc} = 0.84$  in the case of specimen s60-1.

The max-min method consists of the computation of  $h_{max}(r)$ , which is defined as the difference between the maximum and the minimum heights  $h$  within this window, averaged over all possible origins  $x$  of the window [26]:  $h_{max}(r) = \langle \text{Max}\{h(r')\}_{x < r' < x+r} - \text{Min}\{h(r')\}_{x < r' < x+r} \rangle_x$ . For a self-affine profile,  $h_{max}$  is expected to scale as:

$$h_{max}(r) \sim r^{\zeta_{loc}} \quad (5)$$

where  $r$  is the width of the window along  $x$ -axis. For specimen s60-1, we measured a local roughness exponent:  $\zeta_{loc} = 0.89$ .

The third method is a calculation of the power spectrum, *i.e.*, the Fourier transform of the autocorrelation function  $\langle h(x+\Delta x)h(x) \rangle$ . The power spectrum scales for a self-affine profile as [26]:

$$S(k) \sim k^{-(2\zeta_{loc}+1)} \quad (6)$$

where  $k$  is the wave factor. In Figure 4 we show a log-log plot of  $S(k)$  versus  $k$  for specimen s60-1.  $S(k)$  decays with a power law  $k^{-2.78}$  which is consistent with  $\zeta_{loc} = 0.89$ .

The last method used in this study is the averaged wavelet coefficient method [27]. This method consists of the average of the wavelet transform of the profile over the translation factor  $b$ . The averaged wavelet coefficient  $W[h](a)$  scales as

$$W[h](a) \sim a^{\frac{1}{2}+\zeta_{loc}} \quad (7)$$

where  $a$  is the scale factor.

The estimates of the local roughness exponents obtained with these four methods for all specimens are given in Table I. As shown in Table I, the values of the local roughness exponent  $\zeta_{loc}$  calculated by the root mean square method, the max-min method and the power spectrum decrease with the system size  $L$ . Only values obtained from the wavelet analysis seem independent of the

system size. In the following, we show that this deviation is due to measurement and analysis biases and can be corrected.

The reliability of the determination of self-affine exponents has already been studied [27,28]. It has been shown that several artifacts may introduce systematic errors for the estimation of the local roughness exponent. Two types of biases have to be distinguished: those which happen during the geometric measurement of the object and those which are relative to the method of signal analysis.

In our study, profiles are recorded with a needle moving along crack surfaces. For a similar type of measurement [4,28], it has been shown that shape and volume of the needle can induce a geometric filter. When the tip of the needle is a half-sphere, the needle follows hills more correctly than sharp holes. Subsequently the exactness of the measured height is function of the surroundings. It has been found that an increase of the radius of the needle tip induces an increase of the measured roughness exponent (see [28] for more details).

In the case of biases relative to the analysis methods, it has been found that the accuracy of the different methods is sensitive to two parameters : the size of the system (number of recorded points) and the roughness exponent. In our study, the system size strongly evolves from small to big specimens : 360 to 2050 points. In Ref. [28], tests on synthetic profiles generated with self-affine exponent between 0.8-0.9 show that the three methods underestimate the self-affine exponent. The underestimation is larger when the system size decreases. The root mean square method is the most sensitive to this size effect.

Likely both biases exist in this study. In order to evaluate simultaneously the influence of both flaws on local roughness exponents, synthetic profiles are simulated, filtered and analysed. Self-affine profiles are simulated numerically with a *Voss construction* [29] for four values of self-affine exponent : 0.80, 0.85, 0.90 and 0.95. For each exponent, 100 independent profiles are generated. The horizontal step between two consecutive points is  $So = 6.25 \mu\text{m}$  corresponding to the lower cutoff, *i.e.*, the mean thickness of cell walls. Magnification of self-affine profiles corresponds to that measured on experimental profiles. The filter is an under sampling with a sphere of radius  $R = 25 \mu\text{m}$  (*i.e.* size of the experimental needle) every four steps ( $S = 4So = 25 \mu\text{m}$ ). The step  $S$  corresponds to the experimental step  $\Delta x$ . Output exponents are obtained with the four methods (rms, max-min, power spectrum and wavelet analysis) and are given in Table II for different system sizes. From Table II, the corrected values of the experimental  $\zeta_{loc}$  are estimated and given in brackets in Table I. Average of the corrected values of  $\zeta_{loc}$  obtained from the different methods gives the local roughness exponents :  $0.87 \pm 0.07$  for spruce and  $0.88 \pm 0.07$  for pine. Results are consistent with those obtained for brittle materials where  $\zeta_{loc} \approx 0.85$  [6,4,11] and support the conjecture of a universal local roughness exponent.

Our results are different from those obtained by Engöy *et al* [30] who studied the roughness of brittle fractures for different woods. The authors found a local roughness exponent  $\zeta_{loc} = 0.68$  which is characteristic of a two-dimensional fracture. Several reasons might explain this difference. First, direction of propagation crack was perpendicular to fibers while in our setup propagation is parallel to fibers. Second moisture content of tested specimens was around 4% which is significantly lower than that measured in our study (12%). Low moisture content induces micro-cracking in the radial-longitudinal and tangential-longitudinal planes of wood due to drying shrinkage. This mechanism of micro-cracking does not appear in mode I fracture. Micro-cracks induce preferential paths for the macro-crack which modify the scaling properties of fracture surfaces. Third the experimental procedure was strongly different in the study of Engöy *et al* since fracture propagation was unstable contrary to the stable propagation in the present work.

### B. Global roughness and dynamical exponents

As discussed above, the existence of an exponent  $\beta_* \neq 0$  (see Fig. 2) indicates that an anomalous roughening is taking place. To obtain an accurate description of the anomalous scaling, we follow [19,24] and define the scaling function  $g(u)$  as  $g(l/t^{1/z}) = w(l,t)/l^\zeta$ . From Eq.(3),  $g(u)$  is expected to scale like

$$g(u) \sim \begin{cases} u^{-(\zeta-\zeta_{loc})} & \text{if } u \ll 1 \\ u^{-\zeta} & \text{if } u \gg 1 \end{cases} \quad (8)$$

The scaling function  $g$  is computed by data collapses from each profile of a complete crack map, (*i.e.* the set of profiles that describe a single fracture). In Figures 5 and 6 we present the data collapses of  $g(u)$  for all the maps obtained for the three specimen sizes ( $L = 60, 30$  and  $11.25$  mm) of both spruce and pine.

Fig.5(a) is considered as a good example of these data collapses. The quality of the collapse is used for the determination of the dynamical exponent  $z$ . The global exponent  $\zeta$  is obtained from the fit of the scaling function. The time evolution of the height fluctuations at small scales is shown by the nonconstant behavior for  $u \ll 1$ . This regime is fitted by a power law  $g(u) \propto u^{-0.76}$ . Using our previous estimate of the local roughness exponent  $\zeta_{loc} = 0.84$  we obtain the magnitude of the global roughness exponent  $\zeta = 1.60$ . In the particular case of sample s60-1 shown in Fig. 5(a) the best collapse is observed for the dynamical exponent  $z = 5.9$ . Note that estimates of the exponents  $\zeta_{loc} = 0.84$ ,  $\zeta = 1.60$  and  $z = 5.90$  are very consistent with fits obtained from Fig. 2:  $\beta_* = 0.13$  and  $\zeta/z = 0.27$  for this sample.

Data collapses of all maps are presented in Fig.5 and Fig.6 and are in good agreement with a scaling function like (8). For both wood species, global roughness exponent and dynamical exponent are reported in

Tab.I. As shown in Tab.I, global roughness exponents  $\zeta$  are independent of the system size. Average values are  $\zeta = 1.60 \pm 0.10$  for spruce and  $\zeta = 1.35 \pm 0.10$  for pine.

### IV. IMPLICATIONS OF ANOMALOUS SCALING

According to Eq.(3), the roughness is expected to saturate only at times  $t \gg L^z$ , *i.e.*, when the correlation length  $\xi(t) \sim t^{1/z}$  has reached the boundary length,  $\xi_{max} \propto L$ . In this regime the roughness magnitude scales with the system size for any window length even much smaller than the system size  $L$ :

$$w(l, t \gg L^z) \sim l^{\zeta_{loc}} L^{\zeta-\zeta_{loc}} \quad (9)$$

We checked the linear relationship between  $\xi_{max}$  and the system size  $L$  by measuring  $\xi_{max}$ . From the evolution of the roughness  $w(l,t)$  with time (see Fig. 2), the saturation time  $t_{sat}$  is estimated. The correlation length  $\xi_{max}$  is obtained using the relation  $\xi_{max} \propto t_{sat}^{1/z}$ . Values of  $\xi_{max}$  for the different maps are reported in Table I. In figure 7,  $\xi_{max}$  is plotted versus  $L$  for both woods. A linear relationship between  $\xi_{max}$  and the system size  $L$  exists except in the case of spruce for the biggest sample size where the saturation regime is not clearly reached.

In Figure 8, the ratio  $\langle w(l, t \gg \xi_{max}^z) l^{\zeta_{loc}} \rangle_l$  is plotted versus  $L$  for profiles at times  $t \geq (\xi_{max})^z$  for pine specimens. A power law  $L^{\zeta-\zeta_{loc}}$  with exponents determined previously  $\zeta = 1.35$  and  $\zeta_{loc} = 0.80$  is very consistent with data. It confirms the increase of the roughness magnitude with the system size  $L$  even for windows smaller than the system size. In Figure 8  $\langle w(l \ll \xi_{max}, t) / (l^{\zeta_{loc}} \xi_{max}^{\zeta-\zeta_{loc}}) \rangle_l$  versus  $L$  is also plotted (filled symbols) which is expected to be constant.

### V. CONCLUSIONS

In this study we have shown that fracture surfaces of an anisotropic material like wood display an anomalous dynamic scaling of the crack roughness. From different specimen sizes, we have studied the size effects on roughness exponents. It appears that the global roughness exponent is independent of the system size and different for both studied woods. We have obtained  $\zeta = 1.60 \pm 0.10$  for spruce and  $\zeta = 1.35 \pm 0.10$  for pine. The local roughness exponent  $\zeta_{loc}$  shows a deviation according to the system size. However, we argue that this deviation is due to a biased estimate resulting from two independent effects: the number of sampled points and the local filtering resulting from the needle shape during the roughness measurement. Errors due to these biases have to be considered and the corrected values of the local roughness exponents are  $0.87 \pm 0.07$  for spruce and  $0.88 \pm 0.07$  for pine. These results support the conjecture of a universal local roughness exponent for brittle materials. Moreover, we have

shown that it exists a linear relationship between the system size and the maximum correlation length  $\xi_{max}$ . This relation induces a system size dependence in the roughness magnitude at saturation.

Our results can be compared with a recent experiment in granite [19] in which the exponents  $\zeta_{loc} = 0.79$  and  $\zeta = 1.2$  were obtained. We suggest that the global roughness exponent, which seems to be dependent of material, may be a good candidate as an index for characterizing material properties. On the contrary, the local roughness exponent does not seem to change for different materials and might be *universal*. Up to our knowledge, the existing models of cracks are based on the assumption that cracks are truly self-affine, *i.e.*  $\zeta = \zeta_{loc}$ . It is a major interest to find theoretical models of crack interfaces that could incorporate anomalous kinetic roughening in a simple way.

### ACKNOWLEDGMENTS

S.M. wishes to thank E. Bouchaud for very fruitful discussions and encouragement. J.M.L. also thanks M.A. Rodríguez for a careful reading of the manuscript and the European Commission for support.

---

[1] B.B. Mandelbrot, D.E. Passoja, and A.J. Paullay, *Nature* **308**, 721 (1984).  
[2] P. Daguiet, B. Nghiem, E. Bouchaud, and F. Creuzet, *Phys. Rev. Lett.* **78**, 1062 (1997).  
[3] J. Schmittbuhl, S. Roux, and Y. Berthaud, *Europhys. Lett.* **28**, 585 (1994).  
[4] J. Schmittbuhl, F. Schmitt, and C. Scholz, *J. Geophys. Res.* **100**, 5953 (1995).  
[5] J.J. Mecholsky, D.E. Passoja, and K.S. Feinberg-Ringel, *J. Am. Ceram. Soc.* **72**, 60 (1989).  
[6] K.J. Måløy, A. Hansen, E.L. Hinrichsen and S. Roux, *Phys. Rev. Lett.* **68**, 213 (1992).  
[7] E. Bouchaud, G. Lapasset, J. Planès, and S. Navéos, *Phys. Rev. B.* **48**, 2917 (1993).  
[8] J. Planes, E. Bouchaud, and G. Lapasset, *Fractals* **1**, 1059 (1993).  
[9] P. Daguiet, S. Henaux, E. Bouchaud, and F. Creuzet, *Phys. Rev. E.* **53**, 5637 (1996).  
[10] E. Bouchaud, G. Lapasset, and J. Planès, *Europhys. Lett.* **13**, 73 (1990).  
[11] E. Bouchaud, *J. Phys. Cond. Mat.* **9**, 4319 (1997), and references therein.  
[12] J.P. Bouchaud, E. Bouchaud, G. Lapasset, and J. Planès, *Phys. Rev. Lett.* **71**, 2240 (1993).  
[13] T. Halpin-Healy, Y.-C. Zhang, *Phys. Rep.* **254**, 215 (1995), and references therein.  
[14] D. Ertas, M. Kardar, *Phys. Rev. E.* **48**, 1228 (1993).  
[15] D. Ertas, M. Kardar, *Phys. Rev. E.* **49**, R2532 (1994).

[16] J. Schmittbuhl, J.P. Vilotte, S. Roux, and K.J. Måløy, *Phys. Rev. Lett.* **74**, 1787 (1995).  
[17] S. Ramanathan, D. Ertas, and D. Fisher, *Phys. Rev. Lett.* **79**, 873 (1997).  
[18] F. Family, and T. Vicsek, *J. Phys. A* **18**, L75 (1985).  
[19] J.M. López, and J. Schmittbuhl, *Phys. Rev. E* **57**, 6405 (1998).  
[20] J. Krug, *Phys. Rev. Lett.* **72**, 2907 (1994).  
[21] M. Schroeder, M. Siegert, D.E. Wolf, J.D. Shore, and M. Plischke, *Europhys. Lett.* **24**, 563 (1993).  
[22] S. Das Sarma, C.J. Lanczycki, R. Kotlyar, and S.V. Ghaisas, *Phys. Rev. E.* **53**, 359 (1996).  
[23] J.M. López and M.A. Rodríguez, *Phys. Rev. E.* **54**, R2189 (1996).  
[24] J.M. López, M.A. Rodríguez, and R. Cuerno, *Phys. Rev. E.* **56**, 3993 (1997); *Physica A* **246**, 329 (1997).  
[25] *Fracture*, edited by H. Liebowitz (Academic Press, 1969), Volume **5**, Chap. 1.  
[26] J. Feder, *Fractals* (Plenum Press, New York, 1988).  
[27] I. Simonsen, A. Hansen, and O.M. Nes, preprint cond-mat/9707153.  
[28] J. Schmittbuhl, J.P. Vilotte, and S. Roux, *Phys. Rev. E* **51**, 131 (1995).  
[29] R.F. Voss, *Scaling Phenomena in Disorder Systems* (Plenum, New York, 1985).  
[30] T. Engøy, K.J. Måløy, A. Hansen, and S. Roux, *Phys. Rev. Lett.* **73**, 834 (1994).

FIG. 1. Modified tapered double cantilever beam (TDCB) specimen subjected to mode I crack propagation. The crack plane is perpendicular to the tensile axis which corresponds to radial-longitudinal plane of wood (longitudinal direction being the direction of crack propagation). Dimensions are given in mm.

FIG. 2. Roughness (*rms*)  $w(l, t)$  vs. time for a spruce specimen 60 mm wide (s60-1) calculated over windows  $l$  of size ranging from  $l = 0.175$  mm to  $l = 13.975$  mm with size step  $\Delta l = 0.100$  mm. The continuous line (a) corresponds to the fit of the roughness between  $t_{min}$  and  $t_{max}$ ,  $w(l, t) \sim t^{\beta_*}$  for a small window size  $l = 0.175$  mm.  $\beta_* = 0.14$  is obtained. The continuous line (b) is the fit of data for large window size  $l = 13.975$  mm. Its slope 0.26 corresponds to  $\zeta/z$ .

FIG. 3. Roughness (*rms*)  $w(l)$  vs.  $l$  for the profile at the saturated time  $t \gg \xi_{max}^z$  (specimen s60-1). The straight line corresponds to the power law  $w(l) \sim l^{\zeta_{loc}}$  and gives a determination of the local roughness exponent  $\zeta_{loc} = 0.84$ .

FIG. 4. Power spectrum at time  $t_{sat}$  in the case of s60-1 specimen. The straight line has slope -2.78 which is consistent with a power law  $k^{-(2\zeta_{loc}+1)}$  and a local roughness exponent  $\zeta_{loc} = 0.89$ .

FIG. 5. Data collapses for spruce specimens data in three different system sizes. Panel (a), (b), (c) display the data collapses of s60-1, s30-1 and s11-1 specimens which have respectively a size  $L = 60, 30$  and  $11.25$  mm. The non-constant behavior (*i.e.* non zero slope) at small values of  $l/t^{1/z}$  displays the dependence on time of the roughness magnitude, Scalings are in good agreement with the scaling function (Eq.(8)).

FIG. 6. Data collapses for pine specimens of three different system sizes. Panel (a), (b), (c) display the data collapses of p60-1, p30-2 and p11-2 specimens having respectively a size  $L = 60, 30$  and  $11.25$  mm.

FIG. 7. Maximum self-affine correlation lengths  $\xi_{max}$  vs. the system size  $L$  for spruce (circle) and pine (square) specimens. Both spruce and pine show a linear relationship (dashed line) between  $\xi_{max}$  and  $L$ . The determination of  $\xi_{max}$  in the case of spruce and large system size is underestimated owing to the too little duration of the roughness map. The saturation transition was not clearly observable for this sample.

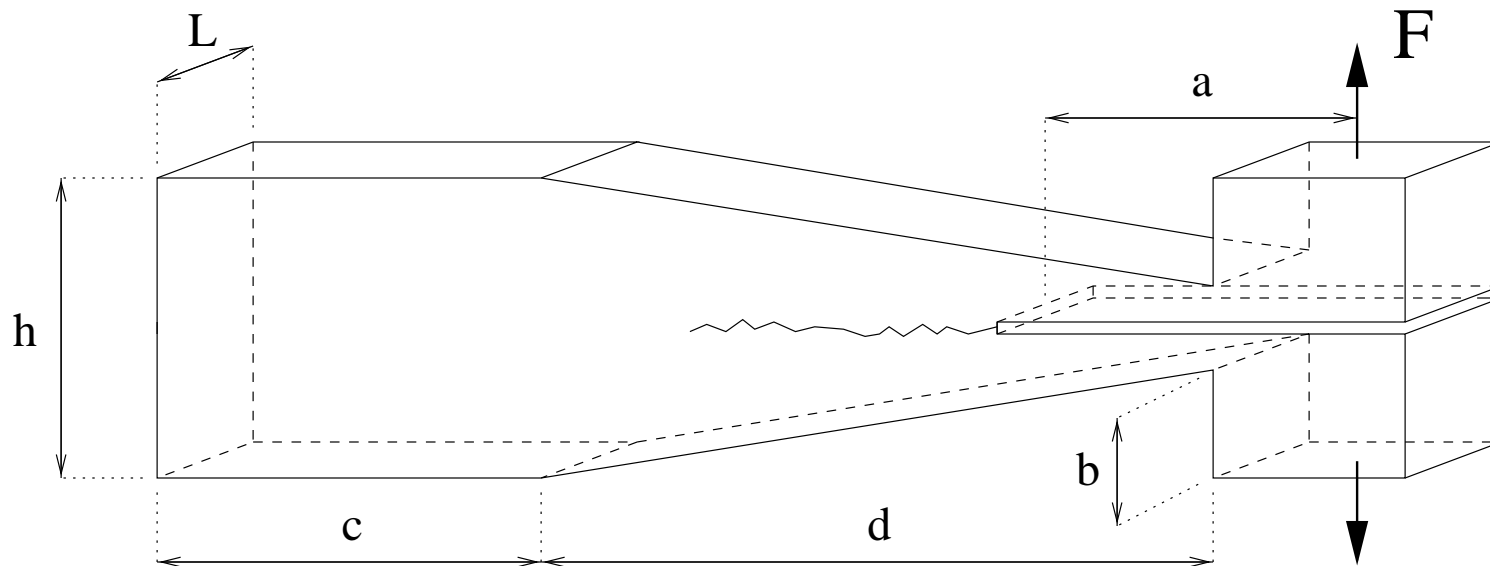
FIG. 8. Size effect on the amplitude of the roughness over profiles at saturation, *i.e.*, at times  $t \geq \xi_{max}^z$ , for pine specimens. Upper symbols correspond to  $\langle w(l \ll \xi_{max}, t) / l^{\zeta_{loc}} \rangle_l$  versus  $L$ : Circle correspond to the specimen of  $L = 60$  mm, squares  $L = 30$  mm, diamonds  $L = 22.5$  mm and triangles  $L = 11.25$  mm. Filled symbols are obtained for  $\langle w(l \ll \xi_{max}, t) / (l^{\zeta_{loc}} \xi_{max}^{\zeta - \zeta_{loc}}) \rangle_l$  versus  $L$ .

TABLE I. Description of the analysed specimens. Local roughness exponents are calculated using the root mean square method, the max-min difference method, the power spectrum, and the averaged wavelet coefficient analysis. Values in brackets are corrected from errors due to measurement and analysis biases.

species	Specimen label	$L$ (mm)	Nb. of profiles	root mean square	Power spectrum	max-min	wavelet analysis	$\zeta$	$z$	$\xi_{max}$ (mm)
spruce	s60-1	60	49	0.84 (0.95)	0.89 (0.86)	0.89 (0.90)	1.00 (0.96)	1.60	5.90	3.90
	s60-2	60	49	0.81 (0.88)	0.85 (0.82)	0.89 (0.90)	0.91 (0.87)	1.55	2.40	4.30
	s60-3	60	43	0.84 (0.95)	0.95 (0.93)	0.87 (0.87)	0.99 (0.95)	1.60	5.60	not sat.
	s30-1	30	48	0.78 (0.84)	0.83 (0.80)	0.83 (0.79)	0.92 (0.87)	1.55	3.50	4.10
	s30-2	30	47	0.79 (0.85)	0.84 (0.81)	0.82 (0.79)	0.89 (0.84)	1.60	2.00	4.20
	s11-1	11.25	22	0.73 (0.80)	0.84 (0.85)	0.83 (0.84)	0.91 (0.84)	1.55	2.50	1.35
	s11-2	11.25	25	0.77 (0.85)	0.84 (0.85)	0.83 (0.84)	0.98 (0.91)	1.60	2.60	1.45
	s11-3	11.25	26	0.79 (0.88)	0.88 (0.93)	0.84 (0.85)	0.95 (0.88)	1.55	2.60	1.40
spruce				$0.88 \pm 0.05$	$0.86 \pm 0.06$	$0.85 \pm 0.07$	$0.89 \pm 0.09$	$1.60 \pm 0.10$		
pine	p60-1	60	45	0.84 (0.95)	0.91 (0.88)	0.90 (0.93)	0.97 (0.93)	1.30	1.90	7.30
	p60-2	60	46	0.81 (0.88)	0.86 (0.83)	0.88 (0.88)	0.90 (0.86)	1.35	2.30	not sat.
	p30-1	30	21	0.84 (0.95)	0.87 (0.85)	0.88 (0.88)	0.99 (0.95)	1.35	2.20	3.85
	p30-2	30	30	0.80 (0.87)	0.81 (0.79)	0.87 (0.87)	0.99 (0.95)	1.30	4.30	not sat.
	p30-3	30	31	0.85 (0.95)	0.83 (0.80)	0.90 (0.95)	0.97 (0.93)	1.40	2.60	3.80
	p30-4	30	31	0.83 (0.92)	0.88 (0.88)	0.89 (0.90)	1.01 (0.96)	1.35	3.90	not sat.
	p11-1	11.25	26	0.75 (0.83)	0.86 (0.88)	0.83 (0.83)	1.03 (0.96)	1.35	3.20	1.40
	p11-2	11.25	27	0.75 (0.83)	0.86 (0.89)	0.83 (0.83)	0.98 (0.91)	1.40	1.80	1.80
	p11-3	11.25	28	0.75 (0.83)	0.82 (0.79)	0.84 (0.84)	0.97 (0.90)	1.30	2.30	not sat.
pine	p22-1	22.50		0.81 (0.89)	0.84 (0.83)	0.85 (0.83)	0.99 (0.94)			
	p22-2	22.50		0.81 (0.89)	0.86 (0.87)	0.85 (0.83)	0.94 (0.88)			
pine				$0.89 \pm 0.05$	$0.84 \pm 0.07$	$0.87 \pm 0.05$	$0.92 \pm 0.08$	$1.35 \pm 0.10$		

TABLE II. Tests of root mean square, power spectrum, max-min difference and wavelet analyses on undersampled and filtered synthetic self-affine profiles which model profiler recording (see text for details). Four system sizes, in terms of number of points are considered. The accuracy of the exponents presented in this table is around 8%.

System size	256 pts				512 pts				1024 pts				2048 pts			
self-affine exponent	0.80	0.85	0.90	0.95	0.80	0.85	0.90	0.95	0.80	0.85	0.90	0.95	0.80	0.85	0.90	0.95
<i>rms</i>	0.72	0.77	0.80	0.82	0.74	0.78	0.81	0.83	0.75	0.79	0.82	0.84	0.75	0.79	0.82	0.84
power spectrum	0.82	0.84	0.87	0.89	0.82	0.85	0.88	0.90	0.83	0.87	0.89	0.91	0.83	0.88	0.93	0.96
<i>max-min</i>	0.81	0.84	0.86	0.89	0.83	0.85	0.88	0.90	0.84	0.86	0.89	0.90	0.84	0.86	0.89	0.91
wavelet analysis	0.87	0.92	0.97	1.02	0.87	0.91	0.96	1.00	0.85	0.90	0.94	0.99	0.84	0.89	0.94	0.99



L	11.25	30	60
a	60	160	320
h	37.50	100	200
b	11.25	30	60
c	90	240	480
d	105	280	560

